

1 **1200 years of Upper Missouri River streamflow reconstructed from tree**
2 **rings**

3 **Justin T. Martin¹, Gregory T. Pederson¹, Connie A. Woodhouse^{2,3}, Edward R.**
4 **Cook⁴, Gregory J. McCabe⁵, Erika K. Wise⁶, Patrick Erger⁷, Larry Dolan⁸, Marketa**
5 **McGuire⁹, Subhrendu Gangopadhyay⁹, Katherine Chase¹⁰, Jeremy S. Littell¹¹,**
6 **Stephen T. Gray¹¹, Scott St. George¹², Jonathan Friedman¹³, Dave Sauchyn¹⁴,**
7 **Jeannine St. Jacques¹⁵, and John King¹⁶**

8 ¹U.S. Geological Survey, Northern Rocky Mountain Science Center, Bozeman, MT, USA

9 ²School of Geography and Development, University of Arizona, Tucson, AZ, USA

10 ³Laboratory of Tree-Ring Research, University of Arizona, Tucson, AZ, USA

11 ⁴Lamont-Doherty Earth Observatory, Palisades, New York, USA

12 ⁵U.S. Geological Survey, Water Resources Division, Denver, Colorado, USA

13 ⁶Department of Geography, University of North Carolina, Chapel Hill, NC, USA

14 ⁷U.S. Bureau of Reclamation, Great Plains Regional Office, Billings, MT, USA

15 ⁸Montana Department of Natural Resources and Conservation, Helena, MT, USA

16 ⁹U.S. Bureau of Reclamation, Technical Service Center, Denver, CO, USA

17 ¹⁰U.S. Geological Survey, Wyoming-Montana Water Science Center, Helena, MT, USA

18 ¹¹U.S. Geological Survey, Alaska Climate Adaptation Science Center, Anchorage AK,
19 USA

20 ¹²Department of Geography, Environment and Society, University of Minnesota,
21 Minneapolis, MN, USA

22 ¹³U.S. Geological Survey, Fort Collins Science Center, Ft. Collins, CO, USA

23 ¹⁴Department of Geography and Environmental Studies, University of Regina, Regina,
24 Saskatchewan, Canada

25 ¹⁵Department of Geography, Planning and Environment, Concordia University, Montreal,
26 Quebec, Canada

27 ¹⁶Lone Pine Research, Bozeman, MT, USA

28
29 Corresponding author: Justin Martin (justinmartin@usgs.gov)

30
31 **Key Words:** Holocene; Paleoclimatology; North America; Tree-rings; Streamflow;
32 Upper Missouri River; Reconstruction

33

34 **Abstract**

35 Paleohydrologic records can provide unique, long-term perspectives on
36 streamflow variability and hydroclimate for use in water resource planning. Such long-
37 term records can also play a key role in placing both present day events and projected
38 future conditions into a broader context than that offered by instrumental observations.
39 However, relative to other major river basins across the western United States, a paucity
40 of streamflow reconstructions has to date prevented the full application of such
41 paleohydrologic information in the Upper Missouri River Basin. Here we utilize a set of
42 naturalized streamflow records for the Upper Missouri and an expanded network of tree-
43 ring records to reconstruct streamflow at thirty-one gaging locations across the major
44 headwaters of the basin. The reconstructions explain an average of 68% of the variability
45 in the observed streamflow records and extend available records of streamflow back to
46 886 CE on average. Basin-wide analyses suggest unprecedented hydroclimatic
47 variability over the region during the Medieval period, similar to that observed in the
48 Upper Colorado River Basin, and show considerable synchrony of persistent wet-dry
49 phasing with the Colorado River over the last 1200 years. Streamflow estimates in
50 individual sub-basins of the Upper Missouri demonstrate increased spatial variability in
51 discharge during the Little Ice Age (~1400-1850 CE) compared with the Medieval
52 Climate Anomaly (~800-1400 CE). The network of streamflow reconstructions
53 presented here fills a major geographical void in paleohydrologic understanding and now

54 allows for a long-term assessment of hydrological variability over the majority of the
55 western U.S.

56

57 **1. Introduction**

58

59 Variability in natural (i.e. unmanaged) streamflow over time reflects the complex
60 interplay of climatic influences such as precipitation and temperature superposed on local
61 attributes including topography, soils, geologic characteristics, and land cover, all of
62 which affect basin hydrology (Lettenmaier and Gan, 1990; McCabe and Wolock, 2011a).
63 Natural streamflow variability is a primary determinant of the amount of surface water
64 available for both societal use and ecological function (Hamlet and Lettenmaier, 1999;
65 Stewart et al., 2005). Because of the substantial influence of natural streamflow
66 variability on water supplies, there has been considerable effort directed towards
67 investigating both the climatic drivers and management implications of hydrologic
68 variability, particularly in the semi-arid to arid American West (Gangopadhyay et al.,
69 2019; Garrick et al., 2008; Lehner et al., 2017; McCabe and Wolock, 2011b; Meko et al.,
70 2007; Woodhouse et al., 2010; Yoon et al., 2015). Observational records in the western
71 U.S. generally span less than 100 years, and are typically inadequate for fully
72 characterizing long-term hydrologic variability including events such as severe and
73 sustained droughts (Woodhouse et al., 2017).

74 In some cases, the limitations imposed by relatively short instrumental streamflow
75 observations can be overcome by extending those records further back in time through
76 the generation of tree-ring based reconstructions of streamflow (Earle and Fritts, 1986;

77 Littell et al., 2016; Meko et al., 2007; Stockton and Jacoby, 1976; Wise, 2010a;
78 Woodhouse, 2001). Historically, most streamflow reconstructions have been focused on
79 basins such as the Upper Colorado River Basin (UCRB) (Hidalgo et al., 2000; Meko et
80 al., 2007; Stockton and Jacoby, 1976; Woodhouse et al., 2006) where surface water is
81 derived primarily from winter precipitation originating in the Pacific Ocean that is
82 subsequently delivered to mid- to high-elevations as snowfall each year (Christensen and
83 Lettenmaier, 2006).

84 Situated to the north and east of the UCRB are the mountain headwaters of the
85 Missouri River, the longest river in North America draining the largest independent river
86 basin in the United States. For the purpose of this study, the Upper Missouri River Basin
87 (UMRB) is defined as the part of the Missouri basin from roughly 105° W longitude to
88 the continental divide, and north to south from the Milk River in Canada to the South
89 Platte River in Colorado (Fig. 1). In contrast to the UCRB, long-term hydrologic
90 variability across the UMRB remains mostly uncharacterized (Ho et al., 2016). With the
91 exception of streamflow reconstructions for several sites in the Yellowstone and Platte
92 basins (Graumlich et al., 2003; Watson et al., 2009; Woodhouse, 2001), no systematic
93 effort aimed at generating a network of long reconstructions of natural streamflow in the
94 UMRB has been successfully undertaken prior to now.

95 Using long-term records of UMRB streamflow, we hope to improve
96 understanding of the potential spatial extent and persistence of high and low streamflow
97 events across the greater U.S. Rocky Mountain region. Synchronous periods of drought
98 in both the UMRB and UCRB during the 1930s, 1950s, late 1980s, and early 2000s
99 suggest that extended hydrologic drought tends to be widespread over much of the

100 northern and southern Rockies. However, this observation runs somewhat counter to
101 evidence that anomalies in both precipitation and snowpack development exhibit a north-
102 south dipole pattern across much of the western U.S. (Dettinger et al., 1998; Pederson et
103 al., 2011; Wise, 2010b). Specifically, observations suggest that northern regions (above
104 ~40 degrees latitude) tend to be anomalously dry when the southern regions are
105 anomalously wet and vice-versa over timescales ranging from inter-annual to multi-
106 decadal (Dettinger et al., 1998; Pederson et al., 2011).

107 Large-scale oceanic/atmospheric teleconnections such as the Atlantic Multi-
108 decadal Oscillation (AMO), Pacific Decadal Oscillation (PDO), and El Niño-Southern
109 Oscillation (ENSO) exhibit significant control over dominant storm tracks, precipitation,
110 and resulting streamflow patterns across the western U.S. (Enfield et al., 2001; Hidalgo
111 and Dracup, 2003; McCabe et al., 2004; Redmond and Koch, 1991). Our understanding
112 of the long-term influence of multidecadal-scale climate variability on streamflow across
113 the western U.S. is again relatively limited since most gage-based estimates of natural
114 streamflow in the western U.S. often only capture one to three full cycles of these
115 important decadal to multi-decadal climate drivers. A multi-century comparison of the
116 AMO and UCRB streamflow since the 1500s suggests that Atlantic sea-surface
117 temperatures have exhibited significant low-frequency control over Colorado river flows
118 when filtered to emphasize the 64-80 year signal in the reconstructed Lee's Ferry record
119 (Nowak et al., 2012). Additionally, a strong 60 year periodicity evident in 820 years of
120 reconstructed precipitation over the Yellowstone plateau indicates that a primary driver
121 of streamflow in the UMRB operates on a similarly low-frequency cycle (Gray et al.,
122 2007). Similar assessments have not been made across the UMRB due to the lack of a

123 network of extended streamflow records, making unclear the potential spatial and
124 temporal influence of these low-frequency climate dynamics on UMRB streamflow and
125 the degree to which they are synchronized with the UCRB.

126 Paleohydrologic records in the western U.S. also help provide a multi-century
127 context for severe and persistent wet and dry conditions. For example, the drought that
128 persisted over the UCRB (Prairie et al., 2008; Udall and Overpeck, 2017; Woodhouse et
129 al., 2010) through the early 2000s was unprecedented over the observational period.
130 Reconstructions of UCRB streamflow suggest that such drought conditions are rare, but
131 have likely occurred in the past (Meko et al., 2007). In fact, in the UCRB, even more
132 sustained periods of drought occurred during the mid 1100s (Woodhouse et al., 2010).
133 However, in the UMRB, we have lacked the extended records necessary to understand
134 recent droughts from a long-term perspective.

135 Finally, recent evidence suggests that significant hydroclimatic changes have
136 occurred across the UMRB in recent decades including a consistent decrease in annual
137 streamflow from the mountain headwater regions (Norton et al., 2014), an increasing
138 trend in March-July temperatures (Wise et al., 2018), reductions in annual snow-to-rain
139 ratios (Wise et al., 2018), increasingly extreme precipitation events (Livneh et al., 2016),
140 and higher flood frequencies (Livneh et al., 2016). Changes such as more extreme
141 precipitation events as well as resulting flood events (Livneh et al., 2016) are consistent
142 with the projected impacts of warming temperatures on precipitation variability
143 (Pendergrass et al., 2017), including areas such as the UMRB. However, in the absence
144 of long-term hydrologic records for the region, it is uncertain if these changes represent a

145 shift to new conditions associated with warmer temperatures in the UMRB or simply a
146 return to previous conditions not represented in the short observational record.

147 Uncertainties in the understanding of long-term streamflow variability in the
148 UMRB, the effects of these uncertainties on water resource management and planning in
149 the basin, and the influence on how we contextualize changing hydro-climatic conditions,
150 highlight a pressing need for extended streamflow estimates for the region. In
151 recognition of this need, we draw on a newly compiled set of naturalized streamflow
152 records for the UMRB and an expanded collection of tree-ring records from the region to
153 explore the following questions: **1)** Is it possible to skillfully reconstruct streamflow
154 records in the UMRB? **2)** What do long-term records reveal about the temporal and
155 spatial characteristics of basin-wide streamflow variability in the UMRB such as the
156 persistence of dry and wet periods and the timing of severe drought in the past? **3)** How
157 do these events compare with droughts and pluvials in the UCRB over past centuries?

158

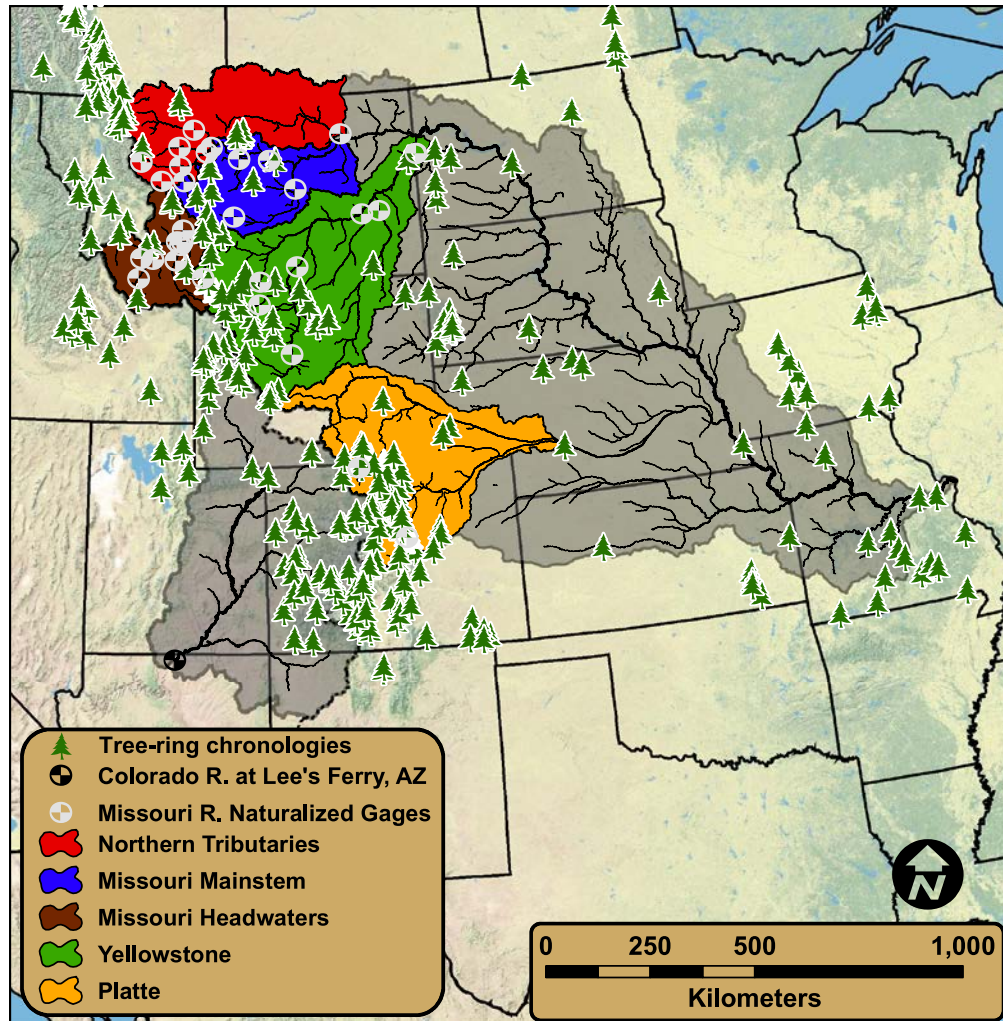
159 **2. Methods and Data**

160

161 2.1 Naturalized streamflow data

162

163 An initial collection of over 300 raw-gaged, and naturalized streamflow records
164 were compiled from 252 gaging locations within Missouri River Hydrologic Region 10
165 (Seaber et al., 1987) and were subsequently screened to produce a set including only the
166 naturalized flow records, or records deemed to reasonably represent natural flow with



167

Figure 1. The 31 reconstructed naturalized Upper Missouri River Basin stream gages, and 374 potential predictor chronologies from 22 different species of trees falling within 250 kilometers of the basin. The Upper Missouri River Basin (UMRB) is shown in color. Its major sub-basins identified through cluster analysis of gage records are also shown. The Upper Colorado River Basin (UCRB) to the south and west, and its major outflow gage at Lee's Ferry AZ are shown for reference.

168 limited modifications from human activity (Falcone, 2011; Slack et al., 1994). The final

169 network of streamflow records for the instrumental period used in generating the

170 paleohydrologic reconstructions contains a total of 31 streamflow records spanning

171 roughly the 1930s through 2010 CE (Brekke et al., 2010; Cary, L.E, Parrett, 1996;

172 Chase, 2014; Gangopadhyay and Pruitt, 2010; Slack et al., 1994) (Fig. 1, Table 1). To
 173 reduce the complexity of the gage network we performed a hierarchical cluster analysis

Table 1. Location and authors of the 31 naturalized streamflow gage records reconstructed across the Upper Missouri River Basin. Grey shading denotes gages used in the Upper Missouri River Basin composite streamflow reconstruction.

174

USGS number	River	Gage Name	Latitude	Longitude	Authors
06016000	Beaverhead	Barretts	45.12	-112.75	Cary, Parrett ^[4]
06025500	Big Hole	Melrose	45.53	-112.70	Erger, Devore, Brekke ^[5]
06287000	Bighorn	St. Xavier	45.32	-107.92	Phillips, Aycock ^a
06207500	Clarks Fork Yellowstone	Belfry	45.01	-109.07	HCDN ^[2]
06073500	Dearborn	Craig	47.20	-112.10	Dolan ^b
06052500	Gallatin	Logan	45.89	-111.44	Erger, Devore, Brekke ^[5]
06036650	Jefferson	Three Forks	45.90	-111.60	Cary, Parrett ^[4]
06114700	Judith	Winifred	47.67	-109.65	Cary, Parrett ^[4]
06041000	Madison	McAllister	45.49	-111.63	Cary, Parrett ^[4]
06042500	Madison	Three Forks	45.82	-111.50	Erger, Devore, Brekke ^[5]
06101500	Marias	Chester	48.31	-111.08	Cary, Parrett ^[4]
06174500	Milk	Nashua	48.13	-106.36	Gangopadhyay ^[7]
06090800	Missouri	Ft. Benton	47.82	-110.67	Cary, Parrett ^[4]
06115200	Missouri	Landusky	47.63	-108.69	Cary, Parrett ^[4]
06054500	Missouri	Toston	46.15	-111.42	Erger, Devore, Brekke ^[5]
06120500	Musselshell	Harlowton	46.43	-109.84	Cary, Parrett ^[4]
06130500	Musselshell	Mosby	46.99	-107.89	Dolan ^b
06620000	North Platte	North Gate	40.94	-106.34	HCDN ^[2]
06326500	Powder	Locate	46.43	-105.31	Chase ^[6]
06023000	Ruby	Twin Bridges	45.51	-112.33	Erger, Devore, Brekke ^[5]
06282000	Shoshone	Buffalo Bill	44.52	-109.10	Phillips, Aycock ^a
06077500	Smith	Eden	47.19	-111.39	Cary, Parrett ^[4]
06707500	South Platte	South Platte	39.41	-105.17	DenverWater ^c
06079500	Sun	Gibson Res	47.60	-112.76	Cary, Parrett ^[4]
06089000	Sun	Vaughn	47.53	-111.51	Cary, Parrett ^[4]
06108000	Teton	Dutton	47.93	-111.55	Cary, Parrett ^[4]
06108800	Teton	Loma	47.93	-110.51	Cary, Parrett ^[4]
06308500	Tongue	Miles City	46.38	-105.85	Chase ^[6]
06259000	Wind	Boysen	43.42	-108.18	Phillips, Aycock ^a
06191500	Yellowstone	Corwin Springs	45.11	-110.79	Chase ^[6]
06329500	Yellowstone	Sidney	47.68	-104.16	Chase ^[6]

^aBureau of Reclamation

^bState of Montana

^cDenver Water

175

176 (clustering based on Ward's method (Murtagh, 1985) of the 31 naturalized streamflow
 177 records over the 40 years common to all gages (1950-1989). Stream gages clustered
 178 neatly into groups reflecting their geographic proximity or location above/below other

179 gages on the same river (Fig. 1). Cluster membership for specific gages then was used
180 for dimension reduction in several analyses described below.

181

182 2.2 Tree-ring data

183

184 A network of climate sensitive tree-ring data exists for the Missouri River basin
185 and surrounding regions that have previously been used to reconstruct snowpack, the
186 summer Palmer Drought Severity Index, and streamflow in other basins (Fig. 1), (Cook et
187 al., 2004; Pederson et al., 2011; Wise, 2010a; Woodhouse et al., 2006). The network
188 contains trees with a diversity of seasonal hydroclimatic sensitivities that are typically
189 related to tree species, elevation, and topographic setting (St. George, 2014; Wettstein et
190 al., 2011). The diversity of climate-growth responses makes this network of tree-ring
191 chronologies suitable for reconstructing streamflow for a network of gages located in a
192 basin that exhibits complex climate and streamflow responses due to a range of factors
193 related to geography, soils, and climate dynamics (Wise et al., 2018). For inclusion in the
194 reconstruction process, all tree-ring records were required to extend prior to the year 1800
195 CE, which resulted in a final dataset of 374 chronologies, 107 of which are new, updated,
196 or were not previously publicly available prior to this research effort. The full set of
197 individual raw ring-width records are now available on the International Tree-Ring Data
198 Bank (ITRDB) hosted by the National Oceanic and Atmospheric Administration
199 (NOAA) National Climatic and Data Center (NCDC) at
200 <https://www.ncdc.noaa.gov/paleo-search/study/26831>.

201 Tree-ring chronologies were constructed from these raw ring-width records by
202 first removing the non-climatic biological growth curve from the individual records (i.e. a
203 process known as “detrending”) following methods Melvin & Briffa, (2008). Removal of
204 geometric tree-growth artifacts and the production of the standardized ring-width indices
205 was performed using standard methods (Cook et al., 2016). Specifically, here we used
206 an age-dependent spline of unconstrained slope with initial stiffness set to 20-years
207 (Melvin et al., 2007). This individual-series detrending method preserves low-frequency
208 climate signals in a similar fashion to detrending with a negative exponential curve, but
209 with some advantages over the juvenile growth years. However, the unconstrained slope
210 of the detrending spline will remove positive monotonic growth trends if present. The
211 final ring-width index (RWI) chronologies were therefore constructed by calculating a bi-
212 weight robust mean from the power-transformed residuals of the individually detrended
213 ring-width series, reducing the potential for trend distortion from end effects that can
214 result from the ratio method of chronology calculation. Variance stabilization was
215 performed using the Rbar method with correction of trend in variance provided by an
216 age-dependent spline. The length of all chronologies was truncated when the number of
217 individual ring-width measurement series in the chronology fell below five.

218

219 2.3 Climate data

220

221 The climate data used were the 4-kilometer (km) by 4-km gridded monthly
222 temperature and precipitation data from the **P**recipitation-elevation **R**egression on
223 **I**ndependent **S**lopes **M**odel (PRISM) dataset (Daly et al., 2008) for water years (October-

224 September) 1900 through 2014 CE. The gridded monthly temperature and precipitation
225 data were used as inputs to a monthly time-step water balance model (MWBM) from
226 McCabe & Wolock, (2011b) to generate additional hydrologic variables related to
227 streamflow. All hydroclimatic variables then were aggregated to U.S. Geological Survey
228 8-digit hydrologic units (HU) (Seaber et al., 1987) for the UMRB. Water balance model
229 parameters used for this study were taken from parameter sets developed in previous
230 studies (McCabe and Wolock, 2011a; Wise et al., 2018), and soil-moisture-storage
231 capacity for each HU was computed using the available water-capacity values from the
232 State Soil Geographic Data Base (STATSGO) dataset by assuming a one-meter rooting
233 depth, U.S. Department of Agriculture, (1994). Additional details regarding the water
234 balance model and evaluation of the model are described in McCabe & Wolock, (2011b).
235 See E.K. Wise et al., (2018) for further information on the verification of input climate
236 data, and additional details on model performance over the Missouri River Basin.

237

238 2.4 Climate informed reconstruction model development

239

240 Streamflow is controlled by a diversity of season-specific climate factors that vary
241 by sub-basin (e.g. precipitation, temperature, snow accumulation and melt) (Dettinger et
242 al., 2004; Hamlet and Lettenmaier, 1999; Lettenmaier and Gan, 1990; Wise et al., 2018).
243 Likewise, in the UMRB the dominant long-lived tree species span a gradient of moisture
244 to energy limitations (St. George, 2014; Wettstein et al., 2011), and often exhibit different
245 dominant seasonal growth responses to moisture availability, none of which perfectly
246 reflect the seasonal controls on streamflow. Due to both the complexity of climate-

247 growth responses of the tree species within and surrounding the UMRB and sub-basin
248 level responses of streamflow to climate (Wise et al., 2018), reconstructing streamflow
249 for a network of gages across the basin therefore requires novel approaches to using tree-
250 ring records as proxies for discharge. Accordingly, here we develop a “climate-
251 informed” methodology for reconstructing streamflow in the UMRB that seeks to match
252 the dominant climate drivers of annual water-year (prior Oct.1 to Sept. 30) streamflow at
253 each gage to the differing climate-growth responses by optimally integrating this
254 information into a regression modeling and reconstruction framework.

255 In this “climate-informed” modeling approach, we screened all tree-ring
256 chronologies for sensitivity to any of nine climate variables known to influence seasonal
257 streamflow: precipitation, temperature, actual evapotranspiration, potential
258 evapotranspiration, soil moisture, annual water balance (precipitation minus potential
259 evapotranspiration), growing season moisture deficit (potential evapotranspiration minus
260 actual evapotranspiration), and cool season accumulated snowpack using observed April
261 1 snow water equivalent (SWE) (original Natural Resource Conservation Service data
262 compiled and presented within Wise et al. 2018), and MWBM April 1 SWE. Any
263 chronology that was not significantly correlated (at a 95 percent confidence level ($p \leq$
264 0.05)) to a particular climate variable was removed from the potential predictor pool
265 associated with that specific climate variable. This approach allowed us to produce
266 subsets of predictor chronologies significantly correlated with each climate variable and
267 arranged by correlation strength.

268 In developing regression models for reconstructing streamflow, we first
269 transformed all streamflow records to be approximately normally distributed using a

270 maximum likelihood estimated power transformation (Box and Cox, 1964) and then used
 271 a best-subsets approach to model selection using the “*regsubsets*” function in R package
 272 “leaps” (Lumley and Miller, 2004). The function performed an exhaustive search of a
 273 pool of potential predictor chronologies and aided in selection of the best model of each
 274 possible number of predictors. The potential predictor pool consisted of a set of up to 45
 275 (computational limit) chronologies representing the most climatically sensitive records
 276 with respect to each of the 9 climate variables tested in the screening process. This
 277 helped to ensure that the set of tree-ring predictors resulting from the model selection for
 278 each model contained a diversity of climate signals important for streamflow. However,
 279 a maximally diverse set of predictors could not be explicitly constrained in the models
 280 because progressively longer models relied on fewer chronologies and thus, a narrower
 281 range of available tree-ring information. To guide the selection of a skillful and
 282 parsimonious model, the Mallows’ Cp statistic (Mallows, 1973) was used to identify the
 283 model with the lowest difference between the statistic and parameter number. Then,
 284 selection between models with similar number of predictors was informed by identifying
 285 the model with the highest adjusted coefficient of determination (R^2). In selecting the
 286 final model, both metrics (i.e. the Cp and R^2) were weighed evenly, which balanced the
 287 potential for over fitting the model with the increased predictive power of multiple
 288 predictors.

289 Once the model was selected, we fit the generic model: $\mu\{streamflow | RWI\} = \beta_0$
 290 $+ \beta_1 chronology_1 + \beta_2 chronology_2 + \dots + \beta_n chronology_n + \varepsilon$, to the transformed
 291 streamflow data, and back-transformed the predicted values. Ninety percent confidence
 292 bounds were estimated using the delta method (Dorfman, 1938) and back transformed in

293 the same way. To extend the length of the streamflow reconstructions we then nested
294 successive “best” fit models forward and backward in time. This was done by
295 successively dropping any chronologies from the predictor pool that did not extend as far
296 back in time as the predicted values of the previous fitted model. These chronologies
297 then were replaced by the next best-correlated chronology in each of the climate screened
298 chronology lists that had sufficient length to extend the next model either forward or
299 backward in time. This procedure of nesting successively longer reconstructions by
300 fitting the best model and then removing any reconstruction length-limiting chronologies
301 was repeated until no chronologies remained in the potential predictor pool.

302 Because a regression reconstruction inherently underestimates the variability of
303 the past due to a certain amount of unexplained variance in each regression model, we
304 adapted the standard approach (Lutz et al., 2012) to restoring variance in a nested
305 reconstruction by scaling the mean and variance of each progressively longer and less
306 skillful model to match that of the best model over the period common to the two. We
307 then similarly scaled the fully nested reconstruction to the target streamflow record over
308 the calibration period of the best model. This approach maximized the length of record
309 over which variance loss in progressively weaker models could be assessed and scaled
310 the full nested reconstruction to the target record using the estimates of the best
311 reconstruction model.

312 All streamflow reconstructions were developed in units of CFS (cubic feet per
313 second). However, any further analyses and figures presented here were based on
314 streamflow anomalies relative to the mean of the naturalized streamflow record from
315 1930 to 2010, or the z-scores of the full reconstruction.

316

317 2.5 Cross-validation of modeled streamflow

318

319 For each nested model used to reconstruct each gage record, we performed cross
320 validation of model performance using both a leave-one-out and split-sample approach
321 with a calibration period consisting of the earlier half of the available observed record
322 and a verification period consisting of the latter half for the split sample method. We first
323 generated full estimates of verification period streamflow from the model fitting process
324 such that each annual value of observed streamflow was not included in the training data
325 used to predict streamflow for that year. Then, based on the leave-one-out approach and
326 using each nested model in each reconstruction, we calculated the R^2 for the observed
327 record explained by the model parameterized only on training data (VRSQ) and did the
328 same for the predictions made using all observed data in the calibration of the model
329 (CRSQ). Following standard methods, and based on the split-sample calibration and
330 verification approach, we also calculated the reduction of error statistic (RE) (Fritts,
331 1976) and the coefficient of efficiency (CE) (Briffa et al., 1988) for each nested model in
332 each reconstruction.

333

334 2.6 Developing a composite record of basin-wide streamflow from individual

335 reconstructions

336

337 To estimate the average basin-wide streamflow history from the individual
338 reconstructions in the network, we reduced the full network to only those gages for which

339 the naturalized records covered the period of 1930-2010 CE (n=17, Table 1 – shaded
340 rows). This ensured that observational data used to calibrate the reconstruction models at
341 these gages included the driest years of the 1930s Dust Bowl drought and the early 2000s.
342 We first averaged the z -scores of the time series of all reconstructions within each
343 regional cluster to define a cluster-average reconstruction. We then averaged these five
344 reconstructions to define the basin-wide composite reconstruction. We report the 90%
345 confidence interval for each year of the basin-wide composite as the simple average of
346 the 90% confidence intervals of the constituent reconstructions. Likewise, the time-
347 varying reconstruction statistics for the nested UMRB composite are reported as the
348 simple average of the statistics for the 17 underlying reconstructions over time. This
349 approach does underestimate the true skill in reconstructing basin-wide average flow.
350 For example, the squared correlation between observed and modeled composite flow is
351 0.91 but the average VRSQ of the constituent reconstructions over the same period =
352 0.69. However, it provides more information about the uncertainty in the underlying
353 records.

354

355 2.7 Spatial and temporal relationships in streamflow, and notable drought events across
356 the UMRB and the UCRB.

357

358 We explored the long-term spatial variability of streamflow both within the
359 UMRB and across the UMRB-UCRB domain by comparing the correlation between the
360 annual streamflow reconstruction for the most substantial gaging location in each of the
361 five UMRB sub-basins (hereafter “main gage”) as well as the reconstruction for the

362 Colorado river at Lee's Ferry AZ (Meko et al., 2007). We examined the low-frequency
363 coherence among these six gage records by fitting 20- and 60-year cubic smoothing
364 splines (Cook and Kairiukstis, 1990) to the annual streamflow reconstructions, then
365 identified the most severe drought periods as the lowest points in the splines.

366 We assessed temporal variability in basin-wide UMRB and UCRB streamflow by
367 examining the agreement of wet and dry phases between the UMRB composite record
368 and the Lee's Ferry reconstruction (Meko et al., 2007). This comparison focused on
369 multi-decadal and longer temporal variability by using a 60-year spline of annual
370 streamflow anomalies with the agreement across the two basins reported as the
371 percentage of years in which the sign of the anomaly is the same.

372 To describe the dominant modes of quasi-periodic variability within and between
373 streamflow records in the UMRB and UCRB, we analyzed the full common period of the
374 reconstructions spanning 800 to 1998 CE by running a bootstrapped multi-taper method
375 (MTM) spectral and spectral coherency analysis (Mann and Lees, 1996), on the UMRB
376 composite and Lee's Ferry reconstructions, as well as the five UMRB sub-basins. We
377 also assessed the strength and stationarity of the dominant modes of streamflow
378 variability between basins using a wavelet analysis (Torrence and Compo, 1998) run on
379 the UMRB composite record and the reconstruction for Lee's Ferry. For all analyses
380 described in section 2.7, z -scores of the full reconstructed streamflow records from 800-
381 1998 were used.

382

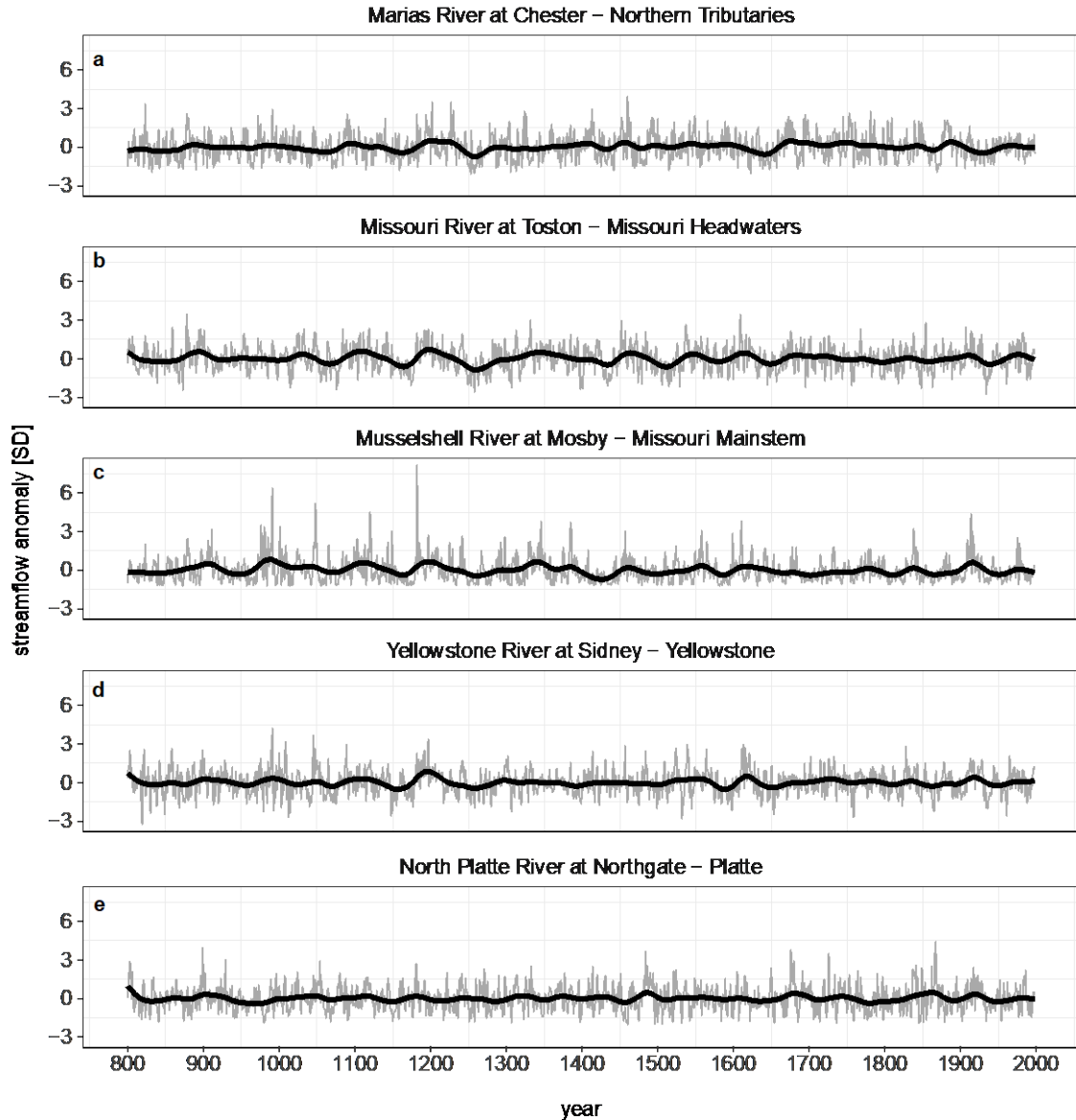
383 **3. Results**

384

385 3.1 Reconstruction modeling results

386

387 Of the 31 reconstructions attempted, it was possible in all cases to skillfully
388 reconstruct natural streamflow with an average verification R^2 (VRSQ) of 0.68. The
389 Bighorn, Madison, Jefferson, Tongue, Dearborn, Judith, Musselshell, mainstem Missouri,
390 as well as the North and South Platte river reconstructions were particularly skillful,
391 (VRSQ > 0.70 for the fifteen gages). Reconstruction models also performed well on the
392 terminal mainstem gages of the Upper Missouri and Yellowstone rivers with VRSQ =
393 0.74 and 0.64 for the Missouri near Landusky and the Yellowstone near Sidney
394 respectively. Several smaller rivers in the eastern portion of the basin such as the Clarks
395 Fork of the Yellowstone and Powder, as well as several of the smaller Missouri
396 tributaries in the northern part of the basin such as the Sun and Teton, proved most
397 difficult to reconstruct. However, all reconstructions retained some level of skill over at



398

Figure 2. Streamflow reconstructions for the most substantial gaging location in each of the 5 sub-basins. Gray lines indicate reconstructed annual values, colored lines show instrumental values overlaid on the reconstructions. Series are smoothed with a 60-year spline (heavy black line). Vertical grey bars denote 60-year periods centered on the lowest point in a 60-year spline. Red bars denote 20-year periods centered on the lowest point in a 20-year spline.

399

400 least the last 700 years, maintaining a correlation with their targets > 0.5 throughout the
 401 length of each nested and variance scaled reconstruction as discussed by McCarroll et al.,
 402 (2015). The reconstructions extended the skillful estimates of streamflow to 886 CE on

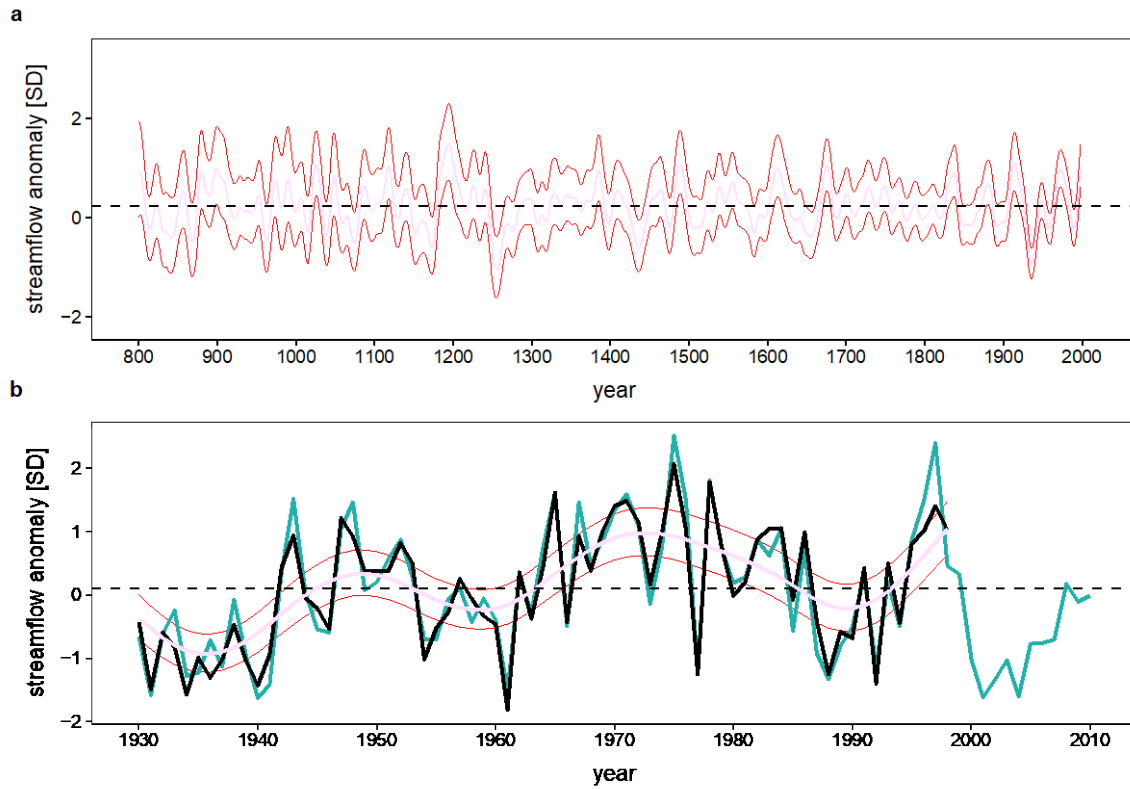
403 average. Streamflow reconstructions for the main gage in each of the 5 UMRB sub-
 404 regions are shown in Figure 2 and cross-validation reconstruction statistics for each gage
 405 reconstruction in the UMRB network are shown in Table 2.

Table 2. Location, calibration coefficient of determination (R^2) (CRSQ), verification R^2 (VRSQ), prediction error (PE) in units of cubic feet per second (CFS), reduction of error statistic (RE), coefficient of efficiency (CE), and start year for the streamflow reconstructions produced for the UMRB. Start year denotes earliest year for which $CRSQ > 0.25$. VRSQ was calculated using a leave-one-out approach while RE and CE were calculated using a split sample approach.

Gage	VRSQ	CRSQ	PE [cfs]	RE	CE	Start Year
6287000	0.85	0.89	679.20	0.85	0.85	722
6041000	0.83	0.87	239.75	0.90	0.79	680
6259000	0.81	0.87	360.48	0.68	0.66	722
6620000	0.80	0.82	122.31	0.79	0.79	379
6042500	0.78	0.84	260.73	0.84	0.54	769
6036650	0.76	0.81	523.53	0.75	0.69	769
6308500	0.75	0.79	136.29	0.82	0.81	989
6115200	0.74	0.80	1957.67	0.81	0.70	769
6114700	0.74	0.80	58.39	0.82	0.78	818
6120500	0.73	0.80	78.64	0.75	0.65	1062
6282000	0.73	0.79	204.17	0.74	0.73	680
6054500	0.73	0.78	968.58	0.80	0.68	680
6073500	0.73	0.80	61.92	0.59	0.55	1044
6707500	0.73	0.78	123.14	0.75	0.75	379
6090800	0.70	0.75	1541.07	0.71	0.71	769
6077500	0.70	0.78	111.62	0.74	0.52	1027
6191500	0.68	0.74	489.99	0.67	0.66	882
6052500	0.68	0.71	208.59	0.69	0.38	680
6101500	0.65	0.75	268.43	0.59	0.58	1125
6025500	0.65	0.70	289.02	0.62	0.61	882
6130500	0.65	0.58	163.55	0.67	0.60	1027
6329500	0.64	0.69	2383.92	0.76	0.75	882
6089000	0.63	0.72	233.74	0.46	0.45	882
6108800	0.59	0.65	68.83	0.63	0.57	1154
6023000	0.59	0.72	63.27	0.79	0.68	1027
6079500	0.58	0.66	216.95	0.56	0.55	1125
6108000	0.56	0.72	57.42	0.50	0.41	1154
6326500	0.55	0.61	195.92	0.63	0.62	1260
6207500	0.53	0.59	160.35	0.65	0.64	769
6016000	0.50	0.62	112.05	0.46	0.45	1260
6174500	0.49	0.65	303.50	0.18	0.18	1104
Average	0.68	0.75	407.84	0.68	0.62	886

407
 408 The full UMRB composite record (Fig. 3a) accurately captures the inter-annual
 409 variation in average observed streamflow anomalies (Fig. 3b) across the UMRB, with the
 410 composite record tracking the observed streamflow average with an $R^2 = 0.91$. The
 411 average reconstruction statistics for the 17 individual gage reconstructions in the
 412 composite record are shown in Fig. 4. Using these statistics for the underlying
 413 reconstructions as a basis for assessing skill in the basin-wide reconstruction, this
 414 composite record skillfully extends estimates of average basin-wide annual streamflow

415 anomalies to 800 CE.



416

Figure 3. (a) The composite streamflow reconstruction for the Upper Missouri River Basin (UMRB)(solid black line) showing a 20-year spline of reconstructed flows (white line), the correspondingly smoothed 90% confidence interval for the spline (pink ribbon), the composite observational record (blue line), and the mean of the reconstructed flows (dashed black line). **(b)** The same as (a) showing the period of the observational record. Y-axis units are standard deviations above and below the 1930-2010 observational mean.

417

418

419 3.2 Spatial relationships within UMRB sub-basin flow and with UCRB streamflow

420

421 Relationships between both
 422 observed and reconstructed streamflow in
 423 the five UMRB sub-basins and the
 424 UCRB at Lee's Ferry most directly
 425 reflect the proximity of one basin to
 426 another with pairs of basins close to one
 427 another displaying the highest
 428 correlations (Figs. 1 and 5). Over the
 429 common period of 1930-1998 CE, the
 430 general spatial pattern of inter-basin
 431 correlations in the network of
 432 reconstructions (Fig 5b) is similar to that
 433 of the observed records (Fig 5a). In
 434 several cases, the strength of the
 435 correlations is enhanced in the
 436 reconstructions (e.g., the dipole between
 437 the northern-most gage and the UCRB),
 438 but for the most part, the correlations in
 439 the reconstructions are similar to those in
 440 the observations.

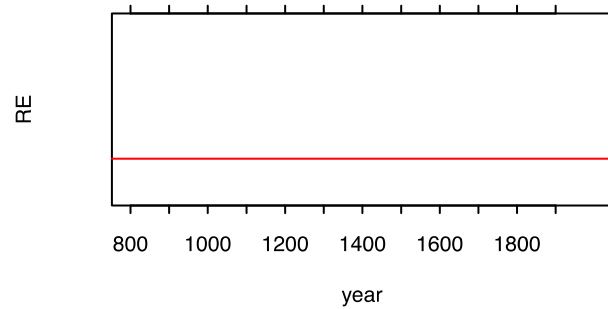
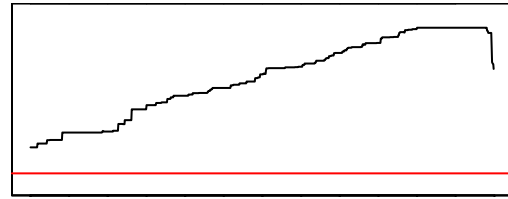


Figure 4. Cross validation statistics for the composite streamflow record showing (a) the calibration coefficient of determination (R^2) (CRSQ), (b) verification R^2 (VRSQ), (c) reduction of error statistic (RE), and (d) coefficient of efficiency (CE).

Figure 4

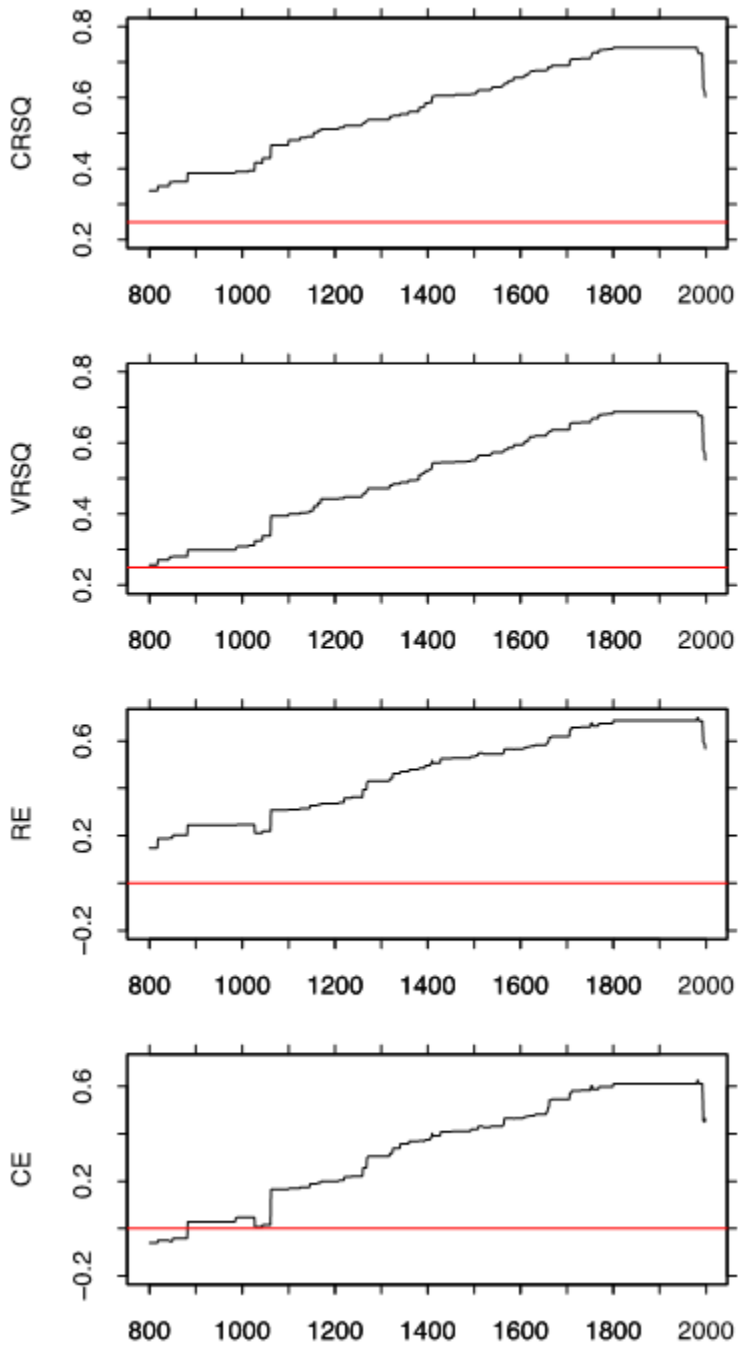


Figure 4. Cross validation statistics for the composite streamflow record showing **(a)** the calibration coefficient of determination (R^2) (CRSQ), **(b)** verification R^2 (VRSQ), **(c)** reduction of error

441 Negative relationships between long-term streamflow variability exist when
442 comparing the basins most distantly situated from each other latitudinally. For example,
443 the UCRB is anti-correlated with the Northern Tributaries region, indicating that the most
444 northern region of the UMRB tends toward dryer conditions when the UCRB tends
445 toward wetter conditions and vice versa.

446 Spatial patterns in the timing of the most severe droughts are also evident from
447 the long-term records (Fig 2). The lowest point in the 60-year spline of annual
448 streamflow indicates a long (multi-decadal to sub-centennial) and relatively sustained
449 period of negative flow anomalies. In the Yellowstone river this point occurs in the mid
450 to late 1100s, closely matching the timing of the most sustained drought period observed
451 in the UCRB (Meko et al., 2007). In the Yellowstone region, this period also marks the
452 lowest point in the 20-year spline of streamflow indicating that the driest years of this
453 sustained drought period were characterized by the deepest decadal to multi-decadal

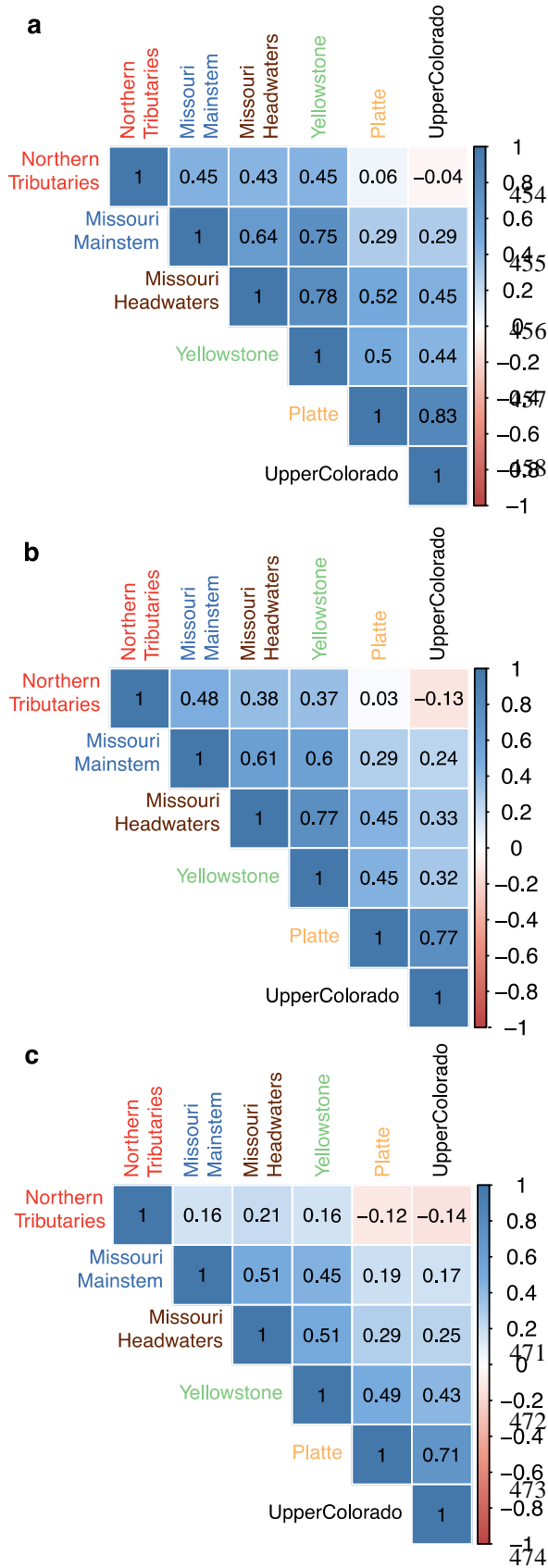
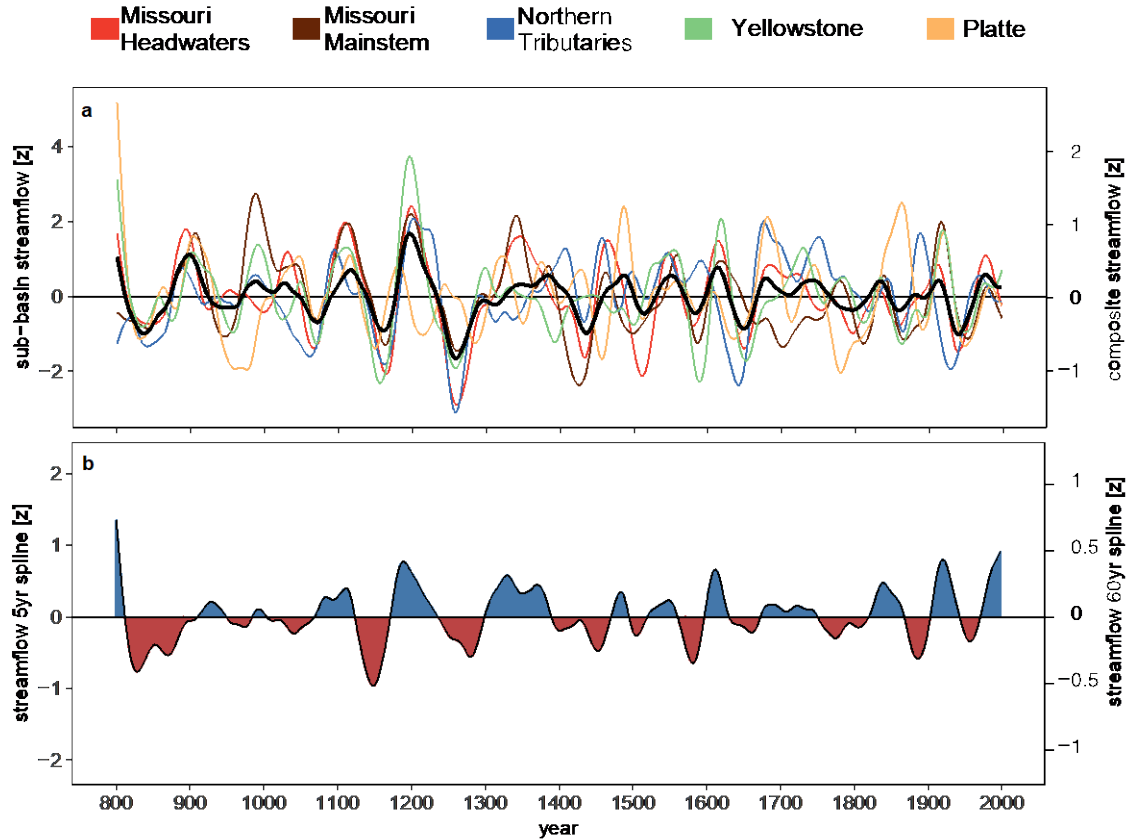


Figure 5. Spatial correlations of (a) observed streamflow (1930-1998), (b) observational period reconstructed streamflow (1930-1998), and (c) full length reconstructed streamflow (800-1998).

departure from average flow conditions. In the Northern Tributaries and Missouri Headwaters regions, the 60-year splines are lowest in the mid 1250s, again highlighting a long-lasting departure from average flows. In the Northern Tributaries, this period was further punctuated by a severe drought period of shorter duration indicated by the lowest point in the 20-year spline. The deepest sub-centennial length drought period in the Missouri Mainstem region (and deepest bi-decadal scale drought in the Headwaters) reached its maximum depth in 1427 CE, centering a period of sustained drought across all three of the uppermost sub-regions of the basin. However, in the Platte this period is centered on the year 1780 CE, closely mirroring the timing of less-severe drought conditions in the neighboring

475 UCRB. The most severe decadal to bi-decadal drought period in the Platte region
476 appears in the late 900s as evidenced by a sharp decline in discharge not evident in other
477 basins.

478 On a basin-wide scale, the most severe drought period in the UMRB was likely
479 centered on the 1250s, where the 60-year spline of the composite streamflow record
480 reaches its lowest point in the entire record. (Fig. 6a). In terms of sustained low-flow



481

Figure 6. 60-year splines of reconstructed streamflow for (a) the UMRB composite (black line) and sub-basins (colored lines) and (b) the UCRB. Gray lines in b show a 5-year spline of UCRB streamflow. Shading in both a & b indicate wet (blue) and dry (red) anomalies identified from the UMRB composite 60-year spline.

482

conditions, this 13th century “megadrought”, reported as the second most widespread

483

period of aridity in the American West over the last 1200 years (Cook et al., 2010), was

484

likely unrivaled over the same time period in the UMRB, with nearly all sub-basins

485

experiencing synchronous and sustained negative departures from average flow

486

conditions (Fig. 6a). However, it also is likely that the depth of drought during the driest

487

years of this multi-decadal event was nearly surpassed by the comparatively brief, but

488

severe Dustbowl drought period of the 1930s, a period during which the 20-year spline of

489

basin-wide flow reached its second lowest level in 1200 years (Fig. 3a).

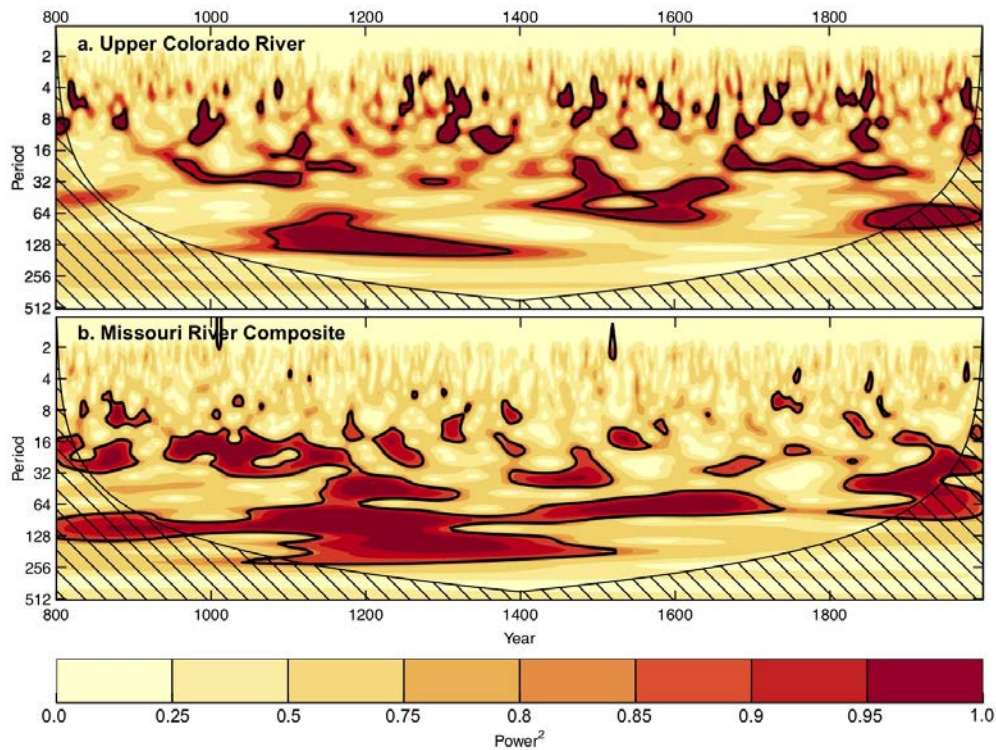
490

491 3.3 Temporal characteristics of long-term basin-wide streamflow variability in the
492 UMRB and the UCRB.

493

494 On a basin-wide scale, streamflow in the UMRB and UCRB are moderately well
495 correlated on an inter-annual basis. Naturalized flows for the UMRB composite correlate
496 with those of the UCRB at Lee's Ferry such that $r = 0.44$ ($p < 0.001$ from 1930-1998 CE
497 while for the reconstructed flows over the same period, $r = 0.43$ ($p < 0.001$). The
498 correlation for the full reconstruction period of 800-1998 CE is very similar, ($r=0.43$, $p <$
499 0.001).

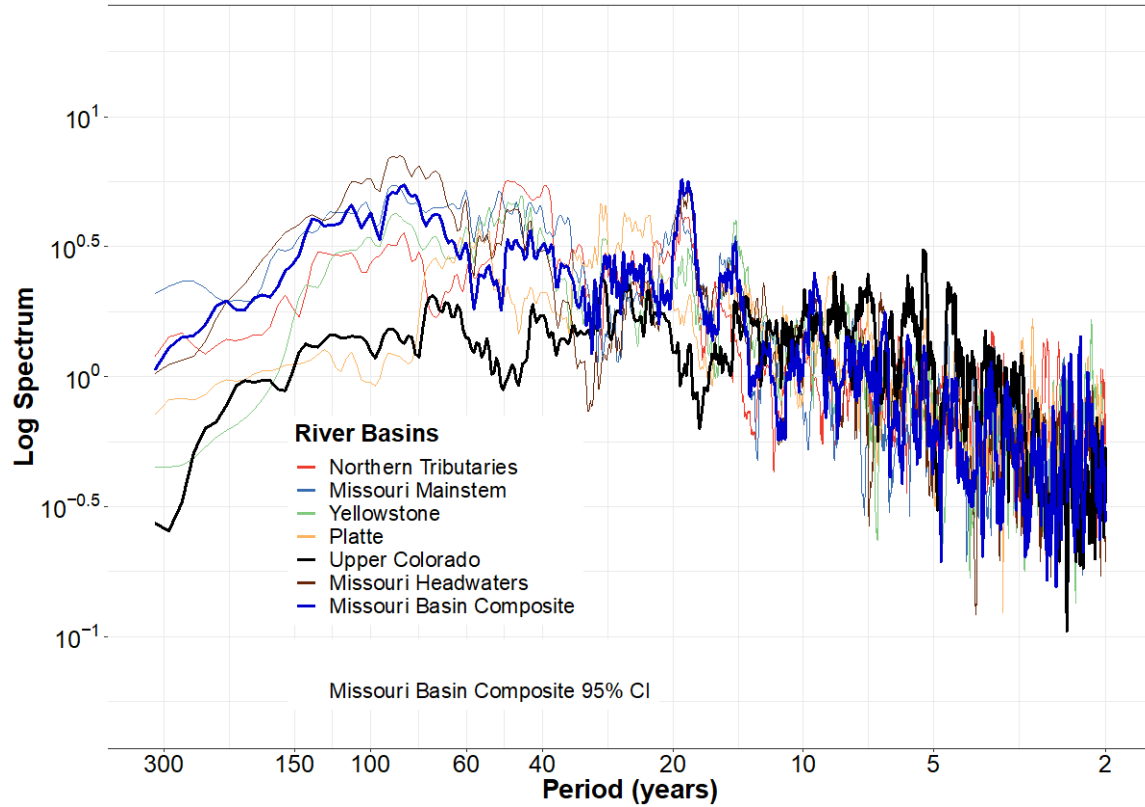
500 In terms of sustained drought and pluvial periods, the magnitude and timing of
501 these different phases is fairly well synchronized across the two basins (Fig 6). Using
502 the 60-year spline as the basis for low-frequency UMRB-UCRB agreement, wet-dry
503 phasing is in agreement (either wet or dry in both basins) 71 percent of the time (Fig 6)
504 over the full record. In both basins, the period from 1100-1400 CE is characterized by
505 increased persistence and amplitude in both wet and dry departures from normal flow
506 conditions while from 1400-1800 CE more rapid shifts between lower amplitude wet and
507 dry phases are generally evident.



508

Figure 7. Wavelet analyses for the (a) UCRB at Lee’s Ferry and (b) UMRB composite time series of water-year flow. The abscissa shows time (water year) and the ordinate is modulating periodicity (period in year). Spectral power is color coded by percentage of each reconstruction spectral power distribution with levels shown on the color bar, and 95% confidence intervals are provided outlining areas of significant power exceeding that of a bootstrapped random autoregressive 1 rednoise distribution. The cross-hatched regions on either end indicate the “cone of influence,” where edge effects become important.

509 Within the frequency domain, both similarities and differences exist between the
 510 UMRB and UCRB. In general, UMRB flow exhibits considerably more persistence than
 511 that of the UCRB with more power evident in lower-frequency modes of variability,
 512 especially during the middle part of the record (~1000 – 1600 CE) (Fig. 7). The MTM
 513 analysis shows that the frequency characteristics of the UMRB are relatively consistent
 514 across its sub-basins, but also highlights the considerable low-frequency power in the
 515 UMRB relative to the UCRB for periods greater than ~20 years (Fig 8). Less power in
 516 the lower frequency signal is also evident in the Platte sub-basin which has the closest
 517 proximity to the UCRB. Conversely, the wavelet and MTM analyses also highlight



518

Figure 8. The Missouri River sub-basins (colored lines), UMRB composite (heavy blue line), and UCRB at Lee's Ferry (heavy black line) streamflow reconstruction multi-taper method (MTM) spectral density estimates shown with the UMRB composite bootstrapped 95 percent (%) confidence intervals (CI) (blue shading). Axes are plotted on a \log_{10} scale with frequency plotted in years (1/frequency) to aid interpretation.

519 considerable power in the 5-10 year periodicity for the UCRB, which is reduced greatly

520 in both the basin-wide and sub-basin records of the UMRB (Figs. 7 & 8).

521

522 4. Discussion

523

524 4.1 Streamflow reconstructions for the UMRB and notable events in the long-term

525 records

526

527 In this study, we present a new network of 31 tree-ring-based reconstructions of

528 streamflow for the Upper Missouri River Basin that span nearly 1200 years and skillfully

529 capture nearly 70% of the observed variation in the gaged records. We also present a
530 composite record of UMRB annual streamflow anomalies built from 17 well-calibrated
531 reconstructions for gaging locations across the five sub-regions of the UMRB. The
532 composite record provides an important estimate of basin-wide streamflow in the Upper
533 Missouri over the past 1200 years. This reconstruction allows, for the first time, a multi-
534 century comparison of streamflow between the UMRB and the UCRB, two neighboring
535 watersheds with headwaters in the US Rocky Mountains.

536 The most notable features of the composite record may be the exceptional pluvial
537 event marking the turn of the 13th century, along with the equally exceptional late-12th
538 and late 13th century drought events that bracketed this major pluvial. A similarly large
539 magnitude and persistent dry-wet-dry swing is evident in the UCRB as well, indicating
540 widespread synchrony in rather extreme hydroclimatic conditions across the Rockies
541 during the Medieval period. This period of persistent, large-magnitude drought and
542 pluvial events in the UMRB and UCRB is then followed by a comparatively quiescent
543 period of low magnitude, short duration flow anomalies during the Little Ice Age (~1400
544 to 1900 CE).

545

546 4.2 Spatial patterns of streamflow in the UMRB and UCRB

547

548 Inter-basin temporal correlations between reconstructed streamflow records for
549 the observed period (1930-1998) are similar to temporal correlations between observed
550 streamflow records for this same period (Fig 5a & b). While the nature of these
551 relationships appears to vary over time (discussed below), the similarity of temporal

552 correlations of inter-basin UMRB observed and reconstructed flows over the common
 553 period (1930-1998 CE) provides additional confidence that the reconstructions capture
 554 not only the temporal dynamics of streamflow in the UMRB over time, but also the
 555 general spatial structure of inter-basin streamflow variability from year-to-year. A
 556 negative relationship between streamflow in the UCRB compared with the Northern
 557 Tributaries is suggested by both observed records ($r = -0.04$, $p=0.73$, $n=69$ – not
 558 significant) and the full reconstructed records ($r = -0.14$, $p<0.001$, $n=1199$). The negative
 559 correlation of streamflow between the extreme northern and southern ends of the region
 560 is consistent with numerous observations of the North to South (N-S) anti-phasing of
 561 precipitation across the Rockies (Dettinger et al., 1998; Pederson et al., 2011; Wise,
 562 2010b). However, the fact that this dipole-like behavior in streamflow is evident only
 563 when comparing the farthest northern and southern ends of the region likely reflects
 564 several underlying characteristics of regional hydroclimate.

565 First, the central latitude of the N-S cool-season precipitation distribution over the
 566 western U.S. (*clat*) ranges primarily between 40 and 45°N over time (Dettinger et al.,
 567 1998; Wise, 2010b). However, the strength of the relationship (as expressed by temporal
 568 Pearson correlation for example) between observed precipitation anomalies and *clat* in a
 569 given year increases as one gets farther away (North or South) from this latitudinal range
 570 (Dettinger et al., 1998). Therefore, because the Northern Tributaries, as well as much of
 571 the Upper Colorado basin, lie farther from the long-term average *clat*, a N-S dipole in
 572 streamflow anomalies resulting from regional precipitation patterns is most likely to be
 573 consistently reflected in comparisons of these most northern and southern river basins.

574 Second, it is likely that regional temperatures play an important role in
 575 modulating the generation of streamflow from precipitation inputs across the UMRB-
 576 UCRB domain, (Woodhouse et al., 2016; McCabe et al., 2017; Udall and Overpeck,
 577 2017) and that this additional influence is expressed in broad spatial patterns that differ
 578 from those of precipitation because of differences in the underlying processes controlling
 579 spatial and temporal variability in each variable.

580 Finally, it is evident from the reconstructed records of streamflow that the amount
 581 of variation between sub-basins of the UMRB is not constant over time but has changed
 582 rather abruptly on several occasions over the last 1200 years. Until roughly 1400 CE,
 583 concurrent with the period of the Medieval Climate Anomaly (MCA), streamflow
 584 dynamics indicated by the 60-year spline of streamflow anomalies appear similar across
 585 all sub-basins (mean pairwise sub-basin inter-annual correlation = 0.32, $p < 0.001$) (Fig.
 586 6). This agreement was particularly strong during the 12th and 13th centuries (mean
 587 pairwise sub-basin inter-annual correlation = 0.35, ($p < 0.001$), a period which saw the
 588 largest sustained low- and high-flow anomalies across both basins in the entire record
 589 (Fig 6a). From ~1400 CE until ~1900 CE concurrent with the period of the Little Ice
 590 Age (LIA), inter-basin agreement was lower than during the MCA (mean pairwise sub-
 591 basin inter-annual correlation = 0.22, $p = 0.16$). Agreement then appears to increase
 592 again around 1900 CE (Fig 6a) (mean pairwise sub-basin inter-annual correlation = 0.43,
 593 $p < 0.05$).

594 A consequence of decreasing agreement is a decrease in the amplitude and
 595 persistence of the basin-wide average flow record. As low flows in one portion of the
 596 basin cancel out high flows in another, the amplitude of the anomaly in the basin-wide

597 record is decreased. Similarly, reconstructions of Pacific Decadal Variability from corals,
598 tree rings, and historical documents have shown that the LIA was characterized by a lack
599 of the low-frequency (pentadecadal) periodicity seen in earlier and later time periods
600 (Biondi et al., 2001; Linsley et al., 2008; MacDonald and Case, 2005; Shen et al., 2006).
601 The transition from the LIA into the 20th century marks the most recent shift to increased
602 amplitude in the low-frequency dynamics of streamflow across the UMRB as well as the
603 UCRB (Fig 6), and corresponds to an increase in the low-frequency component of Pacific
604 Decadal Variability (Biondi et al., 2001; Shen et al., 2006; McCabe-Glynn et al., 2013).
605 Given that temperature is an important variable in delineating the periods of the MCA,
606 LIA, and 20th century, further exploration of how temperature relates to inter-basin
607 agreement and the basin-wide amplitude of anomalies across the UMRB is warranted.

608

609 4.3 Temporal characteristics of long-term streamflow variability in the UMRB and 610 UCRB

611

612 In terms of basin-wide agreement between the UMRB and UCRB, several key
613 features emerged from the 1200-year-long records of streamflow. First, the 60-year
614 splines that characterize the multi-decadal to sub-centennial length departures from
615 average flow are quite similar across the two basins (Fig 6), implying that the processes
616 controlling these gradual changes in regional hydroclimate are likely operating at a broad
617 spatial scale over the Rocky Mountain region. As a result, persistent droughts and pluvial
618 periods in the two basins tend to be in phase most of the time (71%). Secondly, the
619 magnitudes of the low frequency time-series are similar over time with particularly

620 sustained and severe wet and dry periods in both basins tracking closely through the 9th,
 621 12th, and 13th centuries and the tendency toward shorter and less severe departures is
 622 largely mirrored on a basin-wide scale across the UMRB and UCRB during most of the
 623 LIA.

624 Like the UCRB (Meko et al., 2007; Woodhouse et al., 2010), the UMRB record
 625 displays multi-decadal to sub-centennial scale drought and pluvial events during the
 626 Medieval period that are significantly larger and longer than those evident over the period
 627 of the instrumental record (Fig. 6). The most sustained, and consequently largest sub-
 628 centennial scale drought in the UCRB occurred over the middle of the 12th century,
 629 although year-to-year departures were quite moderate over this period. The most severe
 630 and possibly most sustained drought in the UMRB appears during the mid-13th century
 631 and was punctuated by a severely dry decade similar to that which occurred over the
 632 region during the 1930s Dustbowl drought (Fig 3a). Interestingly, in both the UMRB and
 633 UCRB, the wettest period on record as indicated by the 60-year spline (late 12th to mid
 634 13th centuries) falls directly between these two driest periods (Fig 6), suggesting a
 635 roughly 200-year epoch of unprecedented persistence and amplitude in hydroclimatic
 636 variability over the greater Rocky Mountain region during Medieval times.

637 The strong persistence in flow conditions characterizing this period is clearly
 638 evident in the wavelet analyses for both the UMRB and UCRB. Both basins exhibit
 639 significant power in the low-frequency streamflow signal at wavelengths of roughly 128
 640 years (Fig.7). While this low frequency signal is strong in the UCRB from ~1100-1400
 641 CE, it is a much more dominant feature of streamflow record in the UMRB in general,
 642 where a roughly centennial-length cycle is evident throughout the entire MCA, and well

643 in to the early portion of the LIA. In fact, it is clear from both the wavelet (Fig 7) and
 644 MTM spectral (Fig 8) analyses that the UMRB is generally a slower changing basin than
 645 the UCRB. The UMRB displays significant power in the multi-decadal to sub-centennial
 646 modes of variability throughout the 1200-year record and lacks the frequent tendency
 647 towards dominant inter-annual to decadal scale modes of variability evident in the
 648 UCRB.

649 It is important to consider that the estimation of low frequency signals in tree-ring
 650 based proxy records are affected by both inherent features of the tree-ring records
 651 themselves (Cook et al., 1995) and methodological choices made during the chronology
 652 building process (Briffa et al., 1992; Cook et al., 1990; Esper et al., 2002). Considering
 653 this we also compared the frequency characteristics of the comparable Lee's B standard
 654 chronology reconstruction for the UCRB from Woodhouse et al., (2006) to the UMRB
 655 composite in addition to that of Meko et al., (2007) used in this study. We found that in
 656 both cases, the persistence of streamflow across the UMRB was considerably greater than
 657 that of the UCRB. To the extent that the greater reconstruction persistence of the UMRB
 658 relative to that of the UCRB accurately represents true differences in the dynamics of the
 659 basins, this finding aligns with previous work suggesting an ENSO associated, dipolar
 660 patterning of precipitation and drought that is well modulated by slow-changing climate
 661 processes such as the AMO and PDO (McCabe et al., 2004; Wise, 2010b). Because most
 662 of the UMRB lies north of the dipole transition zone of roughly 40-42°N (Wise, 2010b),
 663 persistent precipitation and drought patterns influenced by the long-term phasing of these
 664 persistent climate processes are likely to be more consistent over the UMRB than the
 665 UCRB. This is because the UCRB is approximately bisected by the dipole transition

666 zone, meaning slow changing AMO/PDO influences on streamflow manifested in dipolar
667 weather patterning may be more mixed, and as a result, weaker across the UCRB.

668

669 **5. Conclusion**

670

671 We have reconstructed streamflow for a network of gages across the UMRB back
672 to the early 800s using an updated network of climate-sensitive tree-ring chronologies.

673 The reconstructions are currently being used to provide a long-term perspective on
674 variability in UMRB water supplies, as well as for providing estimates of moisture
675 regime shift probabilities across the western U.S. (Gangopadhyay et al., 2019) and
676 historical drought and pluvial frequencies and durations across the basin to support
677 various planning studies by the U.S. Bureau of Reclamation and partners. In addition,
678 these reconstructions have enabled the first long-term estimate of hydrologic variability
679 across the entire UMRB and an assessment of how individual sub-basins have
680 contributed to that variability over time.

681 In comparing the 1200-year record of streamflow in the UMRB to that of the
682 UCRB it is evident that high-magnitude and long-duration streamflow anomalies not
683 represented in the observed record were widespread across the Rocky Mountain region
684 during the Medieval period, with the most severe drought and pluvial events in both
685 basins occurring in quick succession over the 12th and 13th centuries. The Little Ice Age
686 emerged as a period of increased spatial variability in streamflow between sub-basins
687 within the UMRB. Basin-wide annual streamflow anomalies in both the UMRB and
688 UCRB are moderately correlated over the full length of the record; however, the low

689 frequency dynamics that define prolonged wet and dry departures from average flow
690 conditions are very similar over time. As such, persistent wet and dry periods affecting
691 the UCRB are frequently mirrored in the UMRB, affecting water supplies and
692 challenging flood control operations for a large portion of the country.

693 Finally, the network of reconstructions presented here, in concert with those
694 already available for other river basins across the West, can aid in generating key insights
695 into the long-term nature of spatial and temporal variability of streamflow on a West-
696 wide basis (e.g. Gangopadhyay et al., 2019). In a region heavily dependent on surface
697 water supplies, already struggling to meet increasing water demands in dry years, and
698 facing an uncertain hydrologic outlook due to recent observed changes in temperature
699 and snowpack development (Mote et al., 2018; Portmann et al., 2009), a spatially broad,
700 long-term perspective of streamflow provides an important baseline understanding of
701 hydrologic variability with which to contextualize current and future conditions on the
702 region's rivers.

703

704 **6. Data Availability**

705

706 The naturalized streamflow records used in this study as well as the reconstruction
707 for each record are available online from the USGS
708 (<https://doi.org/10.5066/P9FC7ILX>). The detrended chronologies used in the
709 reconstruction framework are available online from the USGS
710 (<https://doi.org/10.5066/P9FC7ILX>). The full set of individual raw tree-ring-width
711 records are now available on the International Tree-Ring Data Bank (ITRDB) hosted by

712 the National Oceanic and Atmospheric Administration (NOAA) National Climatic and
713 Data Center (NCDC) at <https://www.ncdc.noaa.gov/paleo-search/study/26831>.

714

715 **7. Acknowledgements**

716

717 Research support provided through the National Science Foundation (NSF) Paleo
718 Perspectives on Climate Change (P2C2) Program (Grant No. 1404188, 1403957, and
719 1401549), the NSF Graduate Research Fellowship Program (GRFP; Grant No. 1049562)
720 and the Graduate Research Internship Program (GRIP), the U.S. Bureau of Reclamation
721 WaterSMART Program (Sustain and Manage America's Resources for Tomorrow), the
722 state of Montana Department of Natural Resources and Conservation, and the U.S.
723 Geological Survey Land Resources Mission Area and the North Central Climate
724 Adaptation Science Center. Any findings and conclusions or recommendations expressed
725 in this material are those of the author(s) and do not necessarily reflect the views of the
726 National Science Foundation or any official agency. Coordination of GRIP at USGS is
727 through the Youth and Education in Science programs within the Office of Science
728 Quality and Integrity. Any use of trade, firm, or product names is for descriptive purposes
729 only and does not imply endorsement by the U.S. Government.

730

731

732

733 **References**

734

735 Biondi, F., Gershunov, A., Cayan, D.R., 2001. North Pacific Decadal Climate Variability
736 since 1661. *J. Clim.* 14, 5–10. <https://doi.org/10.1175/1520->

737 0442(2001)014<0005:NPDCVS>2.0.CO;2

738 Box, G., Cox, D., 1964. An analysis of transformations. *J. R. Stat. Soc. B26*, 211–246.

739 Brekke, L.D., Kiang, J.E., Olsen, J.R., Pulwarty, R.S., Raff, D.A., Turnipseed, D.P.,

740 Webb, R.S., White, K.D., 2010. Climate change and water resources management—

741 A federal perspective: U.S. Geological Survey Circular 1331.

742 Briffa, K.R., Jones, P.D., Bartholin, T.S., Eckstein, D., Schweingruber, F.H., Karlen, W.,

743 Zetterberg, P., Eronen, M., 1992. Fennoscandian summers from AD 500:

744 temperature changes on short and long timescales. *Clim. Dyn.* 7, 111–119.

745 Briffa, K.R., Jones, P.D., Pilcher, J.R., Hughes, M.K., 1988. Reconstructing summer

746 temperatures in northern Fennoscandia back to A.D. 1700 using tree-ring data

747 from Scots pine. *Arct. Alp. Res.* 20, 385–384.

748 Cary, L.E., Parrett, C., 1996. Synthesis of natural flows at selected sites in the upper

749 Missouri River Basin, Montana, 1928-89, Montana, USGS Water-Resources

750 Investigations Report 95-4261.

751 Chase, K.J., 2014. Streamflow statistics for unregulated and regulated conditions for

752 selected locations on the Upper Yellowstone and Bighorn Rivers, Montana and

753 Wyoming, 1928–2002. USGS Scientific Investigations Rep. 2014-5115.

754 Christensen, N.S., Lettenmaier, D.P., 2006. A multimodel ensemble approach to

755 assessment of climate change impacts on the hydrology and water resources of the

- 756 Colorado River Basin. *Hydrol. Earth Syst. Sci.* 3, 3727–3770.
757 <https://doi.org/10.5194/hess-11-1417-2007>
- 758 Cook, E.R., Briffa, K.R., Meko, D.M., Graybill, D.A., Funkhouser, G., 1995. The
759 “segment length curse” in long tree-ring chronology development for
760 palaeoclimatic studies. *The Holocene* 5, 229–237.
- 761 Cook, E.R., Briffa, K.R., Shiyatov, S.G., Mazepa, V.S., 1990. Tree-ring standardization
762 and growth-trend estimation, in: Cook, Edward R., Kairiukstis, L.A. (Eds.), *Methods*
763 *of Dendrochronology, Applications in the Environmental Sciences*. Springer, New
764 York, pp. 104–123.
- 765 Cook, E.R., Kairiukstis, L.A., 1990. *Methods of dendrochronology: applications in the*
766 *environmental sciences*. Kluwer Academic Publishers, Boston.
- 767 Cook, E.R., Krusic, P.J., Melvin, T.M., 2016. RCS Signal-Free Batch Processing
768 Program: Version 47(b).
- 769 Cook, E.R., Seager, R., Heim, R.R.J., Vose, R.S., Herweijer, C., Woodhouse, C., 2010.
770 Megadroughts in North America: placing IPCC projections of hydroclimatic change
771 in a long-term paleoclimate context. *J. Quat. Sci.* 25, 48–61.
- 772 Cook, E.R., Woodhouse, C.A., Eakin, M., Meko, D.M., Stahle, D.W., 2004. Long-term
773 aridity changes in the western United States. *Science* (80-.). 306, 1015–1018.
774 <https://doi.org/10.1126/science.1102586>
- 775 Daly, C., Halbleib, M., Smith, J.I., Gibson, W.P., Dogget, M.K., Taylor, G.H., Curtis, J.,
776 Pasteris, P.P., 2008. Physiographically sensitive mapping of climatological
777 temperature and precipitation across the conterminous United States. *Int. J.*
778 *Climatol.* 28, 2031–2064.

- 779 Dettinger, M.D., Cayan, D.R., Diaz, H.F., Meko, D.M., 1998. North-South precipitation
780 patterns in western North America on interannual-to-decadal timescales. *J. Clim.* 11,
781 3095–3111. [https://doi.org/10.1175/1520-0442\(1998\)011<3095:NSPPIW>2.0.CO;2](https://doi.org/10.1175/1520-0442(1998)011<3095:NSPPIW>2.0.CO;2)
- 782 Dettinger, M.D., Cayan, D.R., Meyer, M.K., Jeton, A., 2004. Simulated hydrologic
783 responses to climate variations and change in the Merced, Carson, and American
784 River basins, Sierra Nevada, California, 1900-2099 *. *Clim. Change* 62, 283–317.
785 <https://doi.org/10.1023/B:CLIM.0000013683.13346.4f>
- 786 Dorfman, R., 1938. A Note on the delta Method for Finding Variance Formulae.
787 *Biometric Bull.* 1, 129–137.
- 788 Earle, C.J., Fritts, H.C., 1986. “Reconstructing riverflow in the Sacramento River Basin
789 since 1560”. California Department of Water Resources Report DWR B-55395.
- 790 Enfield, D.B., Mestas-Nunez, A.M., Trimble, P.J., 2001. The Atlantic multidecadal
791 oscillation and its relation to rainfall and river flows in the continental U.S.
792 *Geophys. Res. Lett.* 28, 2077–2080.
- 793 Esper, J., Cook, E.R., Schweingruber, F.H., 2002. Low-frequency signals in long tree-
794 ring chronologies for reconstructing past temperature variability. *Science* (80-.).
795 295, 2250–2253. <https://doi.org/10.1126/science.1066208>
- 796 Falcone, J., 2011. GAGES-II: Geospatial Attributes of Gages for Evaluating Streamflow.
- 797 Fritts, H.C., 1976. *Tree rings and climate*. Academic, San Diego.
- 798 Gangopadhyay, S., McCabe, G., Pederson, G., Martin, J., Littell, J.S., 2019. Risks of
799 hydroclimatic regime shifts across the western United States. *Sci. Rep.* 9, 6303.
800 <https://doi.org/10.1038/s41598-019-42692-y>
- 801 Gangopadhyay, S., Pruitt, T., 2010. Climate Change Analysis for the St . Mary and Milk

- 802 River Systems in Montana. Reclamation Technical Memorandum No. 86-68210–
803 2010-04.
- 804 Garrick, D., Jacobs, K., Garfin, G.M., 2008. Decision making under uncertainty:
805 Shortage, stakeholders and modeling in the Colorado River basin. *J. Am. Water*
806 *Resour. Assoc.* 44, 381–398.
- 807 Graumlich, L.J., Pisaric, M.F., Waggoner, L.A., Littell, J.S., King, J.C., 2003. Upper
808 Yellowstone River Flow and Teleconnections With Pacific Basin Climate
809 Variability During the Past Three Centuries Article. *Clim. Change* 59, 245–262.
810 <https://doi.org/10.1023/A>
- 811 Gray, S.T., Graumlich, L.J., Betancourt, J.L., 2007. Annual precipitation in the
812 Yellowstone National Park region since AD 1173. *Quat. Res.* 68, 18–27.
813 <https://doi.org/10.1016/j.yqres.2007.02.002>
- 814 Gray, S.T., Graumlich, L.J., Betancourt, J.L., Pederson, G.T., 2004. A tree-ring based
815 reconstruction of the Atlantic Multidecadal Oscillation since 1567 A.D. *Geophys.*
816 *Res. Lett.* 31, L12205. <https://doi.org/10.1029/2004GL019932>
- 817 Hamlet, A.F., Lettenmaier, D.P., 1999. Effects of climate change on hydrology and water
818 resources in the Columbia River Basin. *J. Am. Water Resour. Assoc.* 35, 1597–
819 1623.
- 820 Hidalgo, H.G., Dracup, J.A., 2003. ENSO and PDO effects on hydroclimatic variations
821 of the Upper Colorado River Basin. *J. Hydrometeorol.* 4, 5–23.
- 822 Hidalgo, H.G., Piechota, T.C., Dracup, J.A., 2000. Alternative principal components
823 regression procedures for dendrohydrologic reconstructions. *Water Resour. Res.* 36,
824 3241–3249. <https://doi.org/10.1029/2000WR900097>

- 825 Ho, M., Lall, U., Cook, E.R., 2016. Can a paleodrought record be used to reconstruct
826 streamflow?: A case study for the Missouri River Basin. *Water Resour. Res.* 52,
827 5195–5212. <https://doi.org/10.1002/2015WR018444>. Received
- 828 Lehner, F., Wood, A.W., Llewellyn, D., Blatchford, D.B., Goodbody, A.G.,
829 Pappenberger, F., 2017. Mitigating the Impacts of Climate Nonstationarity on
830 Seasonal Streamflow Predictability in the U.S. Southwest. *Geophys. Res. Lett.* 44,
831 12,208–12,217. <https://doi.org/10.1002/2017GL076043>
- 832 Lettenmaier, D.P., Gan, T.Y., 1990. Hydrologic Sensitivities of the Sacramento-San
833 Joaquin, California, to Global Warming. *Water Resour. Res.* 26, 69–86.
- 834 Linsley, B.K., Zhang, P., Kaplan, A., Howe, S.S., Wellington, G.M., 2008. Interdecadal-
835 decadal climate variability from multicoral oxygen isotope records in the South
836 Pacific Convergence Zone region since 1650 A.D. *Paleoceanography* 23, PA2219.
837 <https://doi.org/10.1029/2007PA001539>
- 838 Littell, J.S., Pederson, G.T., Gray, S.T., Tjoelker, M., Hamlet, A.F., Woodhouse, C.A.,
839 2016. Reconstructions of Columbia River streamflow from tree-ring chronologies in
840 the Pacific Northwest, USA. *J. Am. Water Resour. Assoc.* 52, 1121–1141.
841 <https://doi.org/10.1111/1752-1688.12442>
- 842 Livneh, B., Hoerling, M.P., Badger, A.M., Eischeid, J.K., Webb, R.S., 2016. Causes for
843 hydrologic extremes in the Upper Missouri River Basin. NOAA Climate
844 Assessment Report.
- 845 Lumley, A.T., Miller, A., 2004. The leaps Package.
- 846 Lutz, E.R., Hamlet, A.F., Littell, J.S., 2012. Paleoreconstruction of cool season
847 precipitation and warm season streamflow in the Pacific Northwest with applications

- 848 to climate change assessments. *Water Resour. Res.* 48, W01525.
849 <https://doi.org/10.1029/2011WR010687>
- 850 MacDonald, G.M., Case, R.A., 2005. Variations in the Pacific Decadal Oscillation over
851 the past millennium. *Geophys. Res. Lett.* 32, L08703.
852 <https://doi.org/10.1029/2005GL022478>
- 853 Mallows, C.L., 1973. Some comments on Cp. *Technometrics* 15, 661–675.
- 854 Mann, M.E., Lees, J., 1996. Robust estimation of background noise and signal detection
855 in climatic time series. *Clim. Change* 33, 409–445.
856 <https://doi.org/10.1007/BF00142586>
- 857 McCabe, G.J., Palecki, M.A., Betancourt, J.L., 2004. Pacific and Atlantic Ocean
858 influences on multidecadal drought frequency in the United States. *Proc. Natl. Acad.*
859 *Sci.* 101, 4136–4141. <https://doi.org/10.1073/pnas.0306738101>
- 860 McCabe, G.J., Wolock, D.M., 2011a. Independent effects of temperature and
861 precipitation on modeled runoff in the conterminous United States. *Water Resour.*
862 *Res.* 47, W11522. <https://doi.org/10.1029/2011WR010630>
- 863 McCabe, G.J., Wolock, D.M., 2011b. Century-scale variability in global annual runoff
864 examined using a water balance model. *Int. J. Climatol.* 31, 1739–1748.
865 <https://doi.org/10.1002/joc.2198>
- 866 McCabe, G.J., Wolock, D.M., Pederson, G.T., Woodhouse, C.A., McAfee, S., 2017.
867 Evidence that recent warming is reducing upper Colorado river flows. *Earth Interact.*
868 21. <https://doi.org/10.1175/EI-D-17-0007.1>
- 869 McCarroll, D., Young, G.H.F., Loader, N.J., 2015. Measuring the skill of variance-scaled
870 climate reconstructions and a test for the capture of extremes. *Holocene* 25, 618–

- 871 626. <https://doi.org/10.1177/0959683614565956>
- 872 Meko, D.M., Stockton, C.W., 1984. Secular variations in streamflow in the western
873 United States. *J. Clim. Appl. Meteorol.* 23, 889–897.
- 874 Meko, D.M., Woodhouse, C.A., Baisan, C.A., Knight, T., Lucas, J.J., Hughes, M.K.,
875 Salzer, M.W., 2007. Medieval drought in the upper Colorado River Basin. *Geophys.*
876 *Res. Lett.* 34, 1–5. <https://doi.org/10.1029/2007GL029988>
- 877 Melvin, T.M., Briffa, K.R., 2008. A “signal-free” approach to dendroclimatic
878 standardisation. *Dendrochronologia* 26, 71–86.
879 <https://doi.org/10.1016/j.dendro.2007.12.001>
- 880 Melvin, T.M., Briffa, K.R., Nicolussi, K., Grabner, M., 2007. Time-varying-response
881 smoothing. *Dendrochronologia* 25, 65–69.
882 <https://doi.org/10.1016/j.dendro.2007.01.004>
- 883 Mote, P.W., Li, S., Lettenmaier, D.P., Xiao, M., Engel, R., 2018. Dramatic declines in
884 snowpack in the western US. *Clim. Atmos. Sci.* 1, 2. [https://doi.org/10.1038/s41612-](https://doi.org/10.1038/s41612-018-0012-1)
885 [018-0012-1](https://doi.org/10.1038/s41612-018-0012-1)
- 886 Murtagh, F., 1985. Multidimensional Clustering Algorithms, in: *COMPSTAT Lectures 4*.
887 Physica-Verlag, Wuerzburg.
- 888 Norton, P.A., Anderson, M.T., Stamm, J.F., 2014. Trends in Annual, Seasonal, and
889 Monthly Streamflow Characteristics at 227 Streamgages in the Missouri River
890 Watershed, Water Years 1960 – 2011 Scientific Investigations Report 2014 – 5053
891 128. <https://doi.org/10.3133/sir2014505>
- 892 Nowak, K., Hoerling, M., Rajagopalan, B., Zagana, E., 2012. Colorado river basin
893 hydroclimatic variability. *J. Clim.* 25, 4389–4403. <https://doi.org/10.1175/JCLI-D->

894 11-00406.1

895 Pederson, G.T., Gray, S.T., Woodhouse, C.A., Betancourt, J.L., Fagre, D.B., Littell, J.S.,

896 Watson, E., Luckman, B.H., Graumlich, L.J., 2011. The Unusual Nature of Recent

897 Snowpack Declines in the North American Cordillera. *Science* (80-.). 333, 332–

898 336.

899 Pendergrass, A.G., Knutti, R., Lehner, F., Deser, C., Sanderson, B.M., 2017. Precipitation

900 variability increases in a warmer climate. *Sci. Rep.* 7, 1–9.

901 <https://doi.org/10.1038/s41598-017-17966-y>

902 Portmann, R.W., Solomon, S., Hegerl, G.C., 2009. Spatial and seasonal patterns in

903 climate change, temperatures, and precipitation across the United States. *Proc. Natl.*

904 *Acad. Sci.* 106, 7324–7329. <https://doi.org/10.1073/pnas.0808533106>

905 Prairie, J., Nowak, K., Rajagopalan, B., Lall, U., Fulp, T., 2008. A stochastic

906 nonparametric approach for streamflow generation combining observational and

907 paleoreconstructed data. *Water Resour. Res.* 44, W06423.

908 <https://doi.org/10.1029/2007WR006684>

909 Redmond, K.T., Koch, R.W., 1991. Surface climate and streamflow variability in the

910 western United States and their relationship to large-scale circulation indices. *Water*

911 *Resour. Res.* 27, 2381–2399.

912 Seaber, P.R., Kapinos, F., Knapp, G.L., 1987. Hydrologic Unit Maps - Water Supply

913 Paper 2294.

914 Shen, C., Wang, W.C., Gong, W., Hao, Z., 2006. A Pacific Decadal Oscillation record

915 since 1470 AD reconstructed from proxy data of summer rainfall over eastern

916 China. *Geophys. Res. Lett.* 33, L03702. <https://doi.org/10.1029/2005GL024804>

- 917 Slack, J.R., Lumb, A.M., Landwehr, J.M., 1994. Hydro-Climatic Data Network (HCDN)
918 - A USGS Streamflow Data Set for the U.S. for the Study of Climate Fluctuations.
919 St. George, S., 2014. An overview of tree-ring width records across the Northern
920 Hemisphere. *Quat. Sci. Rev.* 95, 132–150.
921 <https://doi.org/10.1016/j.quascirev.2014.04.029>
- 922 Stewart, I.T., Cayan, D.R., Dettinger, M.D., 2005. Changes toward earlier streamflow
923 timing across western North America. *J. Clim.* 18, 1136–1155.
924 <https://doi.org/10.1175/JCLI3321.1>
- 925 Stockton, C.W., Jacoby, G., 1976. Long-term surface-water supply and streamflow trends
926 in the Upper Colorado River basin based on tree-ring analyses. *Lake Powell Res.*
927 *Proj. Bull.*
- 928 Torrence, C., Compo, G.P., 1998. A Practical Guide to Wavelet Analysis. *Bull. Am.*
929 *Meteorol. Soc.* 79, 61–78.
- 930 U.S. Department of Agriculture, 1994: State Soil Geographic (STATSGO) data base:
931 Data use information. USDA Miscellaneous Publ. 1492, 113 pp., n.d.
- 932 Udall, B., Overpeck, J., 2017. The twenty-first century Colorado River hot drought and
933 implications for the future. *Water Resour. Res.* 53, 2404–2418.
934 <https://doi.org/10.1002/2016WR019638>.Received
- 935 Watson, T.A., Anthony Barnett, F., Gray, S.T., Tootle, G.A., 2009. Reconstructed
936 streamflows for the headwaters of the Wind River, Wyoming, United States. *J. Am.*
937 *Water Resour. Assoc.* 45, 224–236. [https://doi.org/10.1111/j.1752-](https://doi.org/10.1111/j.1752-1688.2008.00274.x)
938 [1688.2008.00274.x](https://doi.org/10.1111/j.1752-1688.2008.00274.x)
- 939 Wettstein, J.J., Littell, J.S., Wallace, J.M., Gedalof, Z., 2011. Coherent region-, species-,

- 940 and frequency-dependent local climate signals in northern hemisphere tree-ring
941 widths. *J. Clim.* 24, 5998–6012. <https://doi.org/10.1175/2011JCLI3822.1>
- 942 Wise, E.K., 2010a. Tree ring record of streamflow and drought in the upper Snake River.
943 *Water Resour. Res.* 46, W11529. <https://doi.org/10.1029/2010WR009282>
- 944 Wise, E.K., 2010b. Spatiotemporal variability of the precipitation dipole transition zone
945 in the western United States. *Geophys. Res. Lett.* 37, L07706.
946 <https://doi.org/10.1029/2009GL042193>
- 947 Wise, E.K., Woodhouse, C.A., McCabe, G.J., Pederson, G.T., St-Jacques, J.M., 2018.
948 Hydroclimatology of the Missouri River Basin. *J. Hydrometeorol.* 19, 161–182.
949 <https://doi.org/doi:10.1175/JHM-D-17-0155.1>.
- 950 Woodhouse, C.A., 2001. A tree-ring reconstruction of streamflow for the Colorado Front
951 Range. *J. Am. Water Resour. Assoc.* 37, 561–569.
- 952 Woodhouse, C.A., Gray, S.T., Meko, D.M., 2006. Updated streamflow reconstructions
953 for the Upper Colorado River Basin. *Water Resour. Res.* 42, W05415.
954 <https://doi.org/10.1029/2005WR004455>
- 955 Woodhouse, C.A., Lukas, J.J., Morino, K., Meko, D.M., Hirschboeck, K.K., 2017. Using
956 the past to plan for the future-the value of paleoclimate reconstructions for water
957 resource planning, in: Miller, K.A., Hamlet, A.F., Kenney, D.S., Redmond, K.T.
958 (Eds.), *Water Policy and Planning in a Variable and Changing Climate*. CRC Press,
959 Boca Raton, FL, pp. 161–182. <https://doi.org/10.1201/b19534>
- 960 Woodhouse, C.A., Meko, D.M., MacDonald, G.M., Stahle, D.W., Cook, E.R., 2010. A
961 1,200-year perspective of 21st century drought in southwestern North America.
962 *Proc. Natl. Acad. Sci.* 107, 21283–21288. <https://doi.org/10.1073/pnas.0911197107>

- 963 Woodhouse, C.A., Pederson, G.T., Morino, K., McAfee, S.A., McCabe, G.J., 2016.
964 Increasing influence of air temperature on upper Colorado River streamflow.
965 Geophys. Res. Lett. 43, 2174–2181. <https://doi.org/10.1002/2015GL067613>
966 Yoon, J.H., Wang, S.Y.S., Gillies, R.R., Kravitz, B., Hipps, L., Rasch, P.J., 2015.
967 Increasing water cycle extremes in California and in relation to ENSO cycle under
968 global warming. Nat. Commun. 6, 1–6. <https://doi.org/10.1038/ncomms9657>
969